ELSEVIER

Nuclear Engineering and Design 206 (2001) 351–362

Nuclear Engineering and Design

www.elsevier.com/locate/nucengdes

Crack detection and sizing technique by ultrasonic and electromagnetic methods

Ichiro Komura [a,*], Taiji Hirasawa [a], Satoshi Nagai [a], Jun-ichi Takabayashi [b], Katsuhiko Naruse [c]

[a] *Toshiba Corporation, Power & Industrial Systems R&D Center 1–9, Suehiro-cho, Tsurumi-ku, Yokohama, 230-0045, Japan*
[b] *Toshiba Corporation, Keihin Products Operations, 2-4, Suehiro-cho, Tsurumi-ku, Yokohama, 230-0045 Japan*
[c] *Toshiba Corporation, Isogo Nuclear Engineering Center, 8, Shinsugita-cho, Isofo-ku, Yokohama, Japan*

Abstract

Improvements in defect detection and sizing capabilities for non-destructive inspection techniques have been required in order to ensure the reliable operation and life extension of nuclear power plants. For the volumetric inspection, the phased array UT technique has superior capabilities for beam steering and focusing to objective regions, and real-time B-scan imaging without mechanical scanning. In contrast to the conventional UT method, high-speed inspection is realized by the unique feature of the phased array technique. A 256-channel array system has developed for the inspection of weldment of BWR internal components such as core shrouds. The TOFD crack sizing technique also can be applied using this system. For the surface inspection, potential drop techniques and eddy current techniques have been improved, which combined the theoretical analysis. These techniques have the crack sizing capability for surface breaking cracks to which UT method is difficult to apply. This paper provides the recent progress of these phased array and electromagnetic inspection techniques.

1. Introduction

For a long time in Japan, the rules for nuclear safety have not accepted the flaws in the major components of nuclear power plants, in contrast to ASME Sec. XI in 1974. At that time, the structures or components in which flaws were detected by non-destructive examinations, have been repaired or replaced. Recently, this situation has been changed to accept the operation of flawed structures or components with the appropriate analysis for flaw growth by fracture mechanics. A draft of new maintenance standard was proposed by JAPEIC (Japan Power Engineering and Inspection Corporation) in 1996, and this new standard has been published as the JSME (Japan Society of Mechanical Engineers)

* Corresponding author. Tel.: +81-45-5106681; fax: +81-45-5001429.
E-mail address: ichiro.komura@toshiba.co.jp (I. Komura).

0029-5493/01/$ - see front matter
PII: S0029-5493(00)00421-0

standard under the guidance of MITI (Ministry of International Trade and Industry).

This new standard has a critical flaw size to be evaluated in each component of power plants, and flaws larger than the critical size should be analyzed whether the component is safe until the next in-service inspection or not. Therefore, it becomes very important that the detection capability for the flaws larger than the above-mentioned critical size should be insured, and that the improvement of flaw sizing capabilities for the evaluation that the detected flaw is larger than above-mentioned critical size or not.

Under these requirements, the phased array UT technique has been improved, as have volumetric inspection and crack sizing techniques and electromagnetic techniques (potential drop technique and eddy current technique).

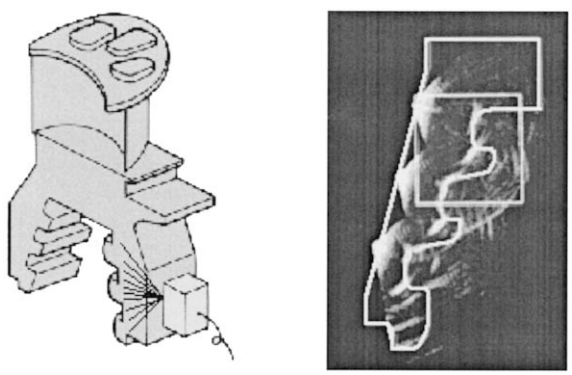

Fig. 1. One of the advantages of phased array for distinguishing the defect echo from the geometrical noise echo.

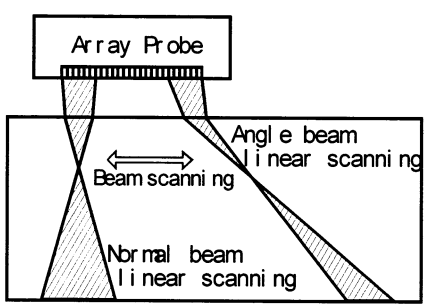

Fig. 2. Water gap phased array method.

2. Crack detection and sizing by phased array technique

2.1. Advantages of the phased array technique and its previous application

The phased array UT technique is both useful and effective (Uchida et al., 1984). One of the typical features of the phased array technique is its real-time imaging capability by using the beam scanning and beam steering function. This function enables a high-speed inspection with minimum use of mechanical scanning, and easy discrimination of defect echo from the geometrical reflections in the complicated shape of examined components, as shown in Fig. 1 (Komura et al., 1985, 1986). Another typical feature of the phased array technique is the use of longitudinal wave and beam focusing for the desired direction and depth (Fischer et al., 1988; Wustenberg et al., 1988). These features assist in detecting defects in and around the weldment of austenitic stainless steel.

The most effective application of these unique features of phased array technique is the immersion or water-gap examination method. In this method, an array probe is set up over the surface under examination with the appropriate distance, and the transmitted ultrasonic beam is scanned along the array elements with the given incidence angle, as shown in Fig. 2 (Komura et al., 1996). Then, the ultrasonic B- scan image, normal beam or angle beam linear scanning image, is obtained without mechanical probe scanning. Furthermore, the sound beam incidence at the surface is barely affected by the surface curvature and unevenness, because of no uncertainty of probe contact compared to the direct contact method.

Fig. 3 shows a schematic illustration of previous applications of the water gap phased array technique developed as the technique for an in-service inspection of the CRD Housing/Stub-tube weldment BWR power plant. In this case, the array probe, with 64-channel array elements, element dimensions of 0.8×10.0 mm, a frequency of 2.0 MHz, and an immersion-type matching layer, was set up in the stub-tube along the axial direction. Normal beam linear scanning operation and one-directional 45° angle beam linear scanning opera-

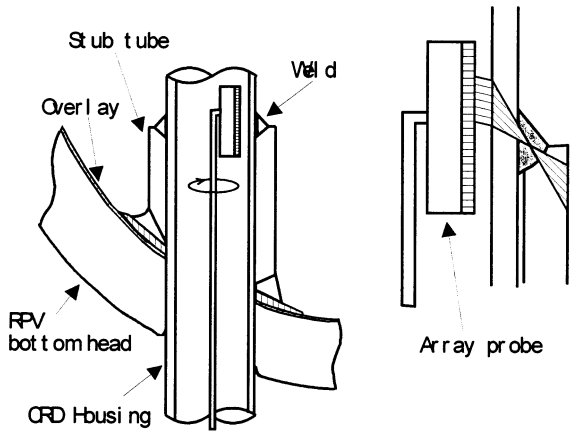

Fig. 3. Application of water gap phased array on the CRD housing and stub-tube weldment.

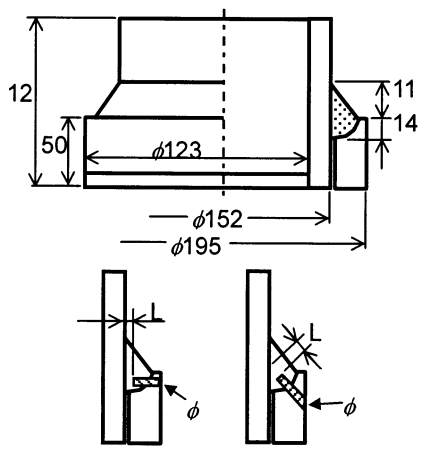

No.	1	2	3	4	5	6	7	8	9
L mm	0	0	0	7	7	7	14	14	14
φ m	2.0	2.8	4.0	2.0	2.8	4.0	2.0	2.8	4.0

Fig. 4. Mock-up specimen for CRD Housing/Stub-tube weldment.

tions were conducted simultaneously. The entire inspection of circumferential weldment was completed only by the rotating mechanical scanning, because the ultrasonic beam scanning for axial direction was carried out electrically.

After the basic experiment for the beam control condition, the defect-detection capabilities were examined on the CRD Housing welded mock-up specimen shown in Fig. 4 by both normal and angle beam scanning operations. Fig. 5 shows the typical B-scan results by normal beam scanning for the flat bottom holes, which are prepared perpendicularly to the pipe wall and have a diameter of 2 mm. In these results, the 2 mm diameter flat bottom holes have a different depth, and each B-scan image is normalized by defect echo amplitude. The flat bottom holes are clearly distinguishable.

2.2. Development of the 256ch phased array system and its application

Ultrasonic examination of a thick plate can be expected to be much more effective with the phased array technique rather than for the above-mentioned thin plate, because the phased array technique leads to a reduction of a large amount of rectangular mechanical scanning, as shown in Fig. 6. Thus, the water gap phased array technique has been examined for an inspection of the core shroud of the BWR internal component. In this case, a newly developed 256-channel array probe has been set up over the weldment with the

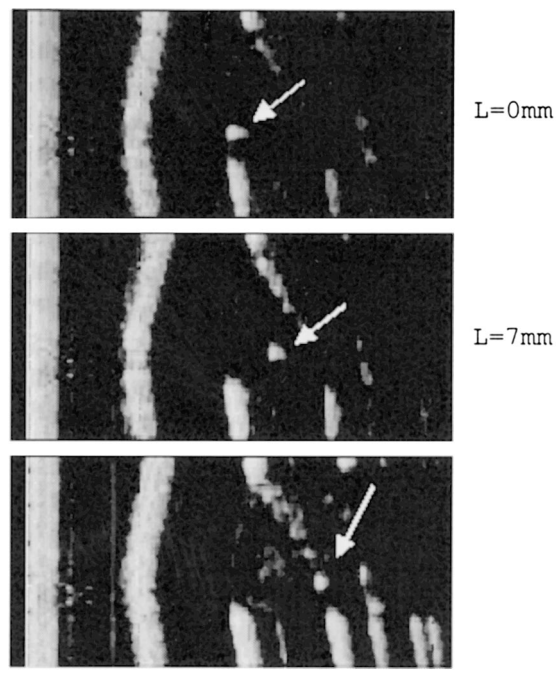

Fig. 5. Results of normal beam linear scanning operation for CRD Housing/Stub-tube welded specimen.

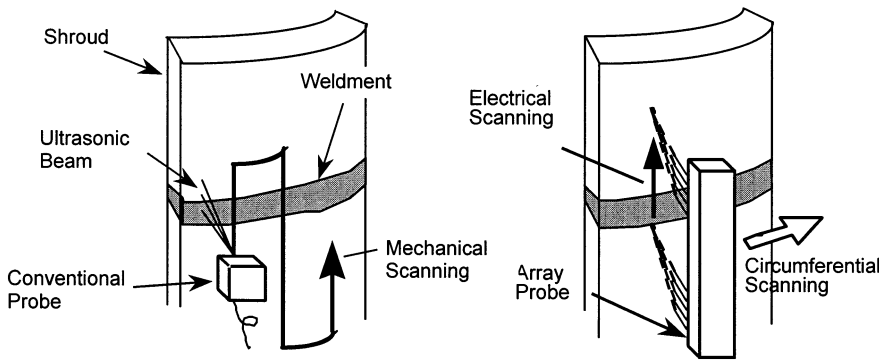

Fig. 6. Difference between conventional UT and water gap phased array UT for the inspection of the core shroud weldment.

water gap of 15 mm. Simultaneous B-scan imaging for three different beam directions, which is normal beam inspection and angle beam inspections from opposite sides of the weldment, can be carried out. Only mechanical scanning along the weld line is required for a complete inspection of the weldment.

Fig. 7 shows the newly developed 256-channel array probe, and Fig. 8 shows the 256ch phased array UT system. Table 1 shows the specifications of this system. The configuration of the CRT display in the on-line mode is described in Fig. 9. Three side-view B-scope images with different beam directions are displayed simultaneously. A C-scope image, end-view B-scope image, and three A-scope waveforms can be displayed.

The ultrasonic beam focusing characteristics of this system were examined. Fig. 10 shows the beam characteristics for $\phi 3.2$ SDH at a depth of 1/4 t and 3/4 t position, and each figure shows the results with the normal beam and angle beam of 45° and $-45°$. The results with the angle beam of 45° is the through-weld result, and the echo amplitude is about 6 dB lower than the angle of $-45°$. In this condition, the defect-detection and sizing capabilities have been examined on the specimens that had EDM slots and artificially induced SCCs. SCC had been induced under the conditions of the BWR environment in the autoclave. Fig. 11 shows the result of crack depth sizing for the EDM slots prepared from the far surface of specimens. A good correlation between the actual slot size and the measured size by phased array UT is observed. Fig. 12 shows one of the typical imaging results on SCC specimen.

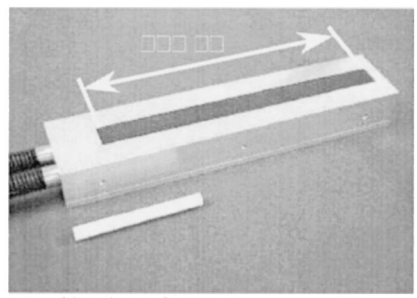

Fig. 7. 256ch phased array probe

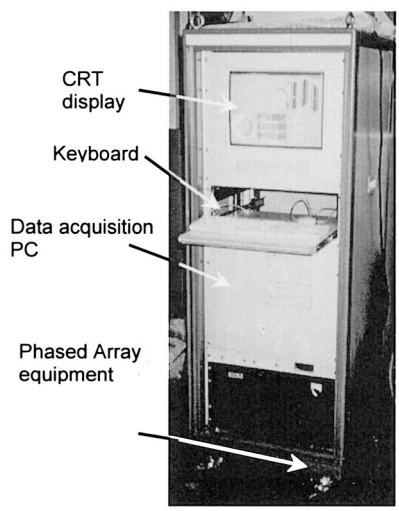

Fig. 8. 256ch phased array system

Table 1
Specification of the array system

Pulser/receiver
Pulse voltage: 50–400 V
Pulse rise time: 7 ns
Number of channels: 256
Number of control channels: 32
Delay-time resolution: 10 ns
Maximum gain: 74 dB
A/D converter
Number of channels: 32
Sampling rate: 20 MHz

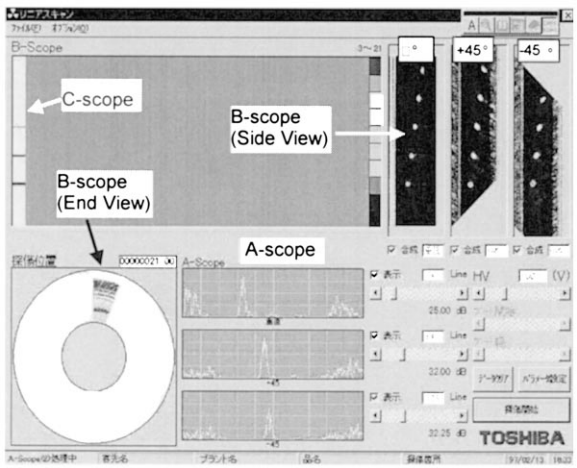

Fig. 9. On-line mode CRT display of the newly developed 256-ch phased array system

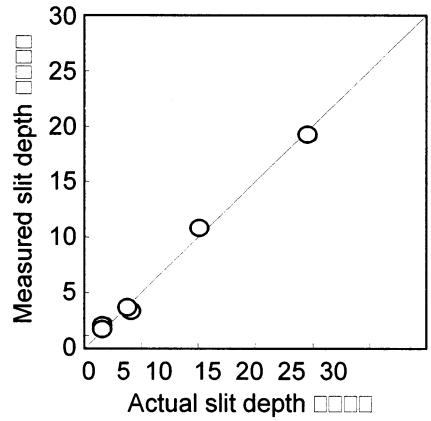

Fig. 11. Slit depth sizing accuracy by the tip diffraction echo method.

In this specimen, the tip of SCC has branched. The difference of three B-scope images from different beam direction is observed. Thus, it has been shown that the inspection results from different beam direction by phased array system are useful in obtaining the correct information about the size and shape of branched SCC.

2.3. Phased array TOFD technique by 256ch array system

One of the unique techniques of phased array applications is the TOFD B-scan inspection without mechanical probe scanning. This technique has been named "Phased Array TOFD" and is

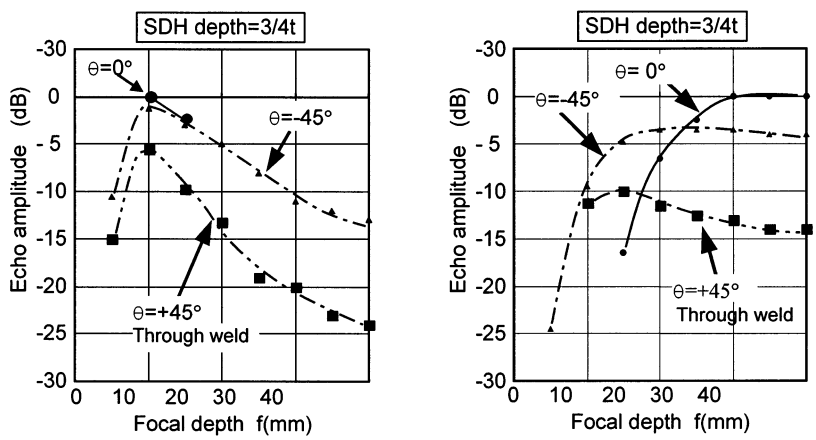

Fig. 10. Ultrasonic beam focusing characteristics on ϕ3.2 mm SDH at different depths.

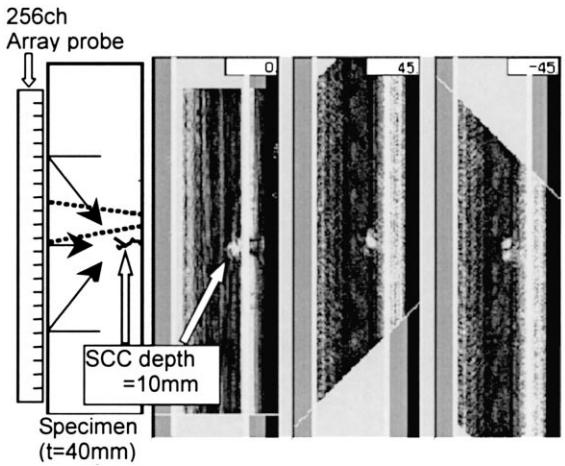

Fig. 12. Typical imaging results of SCC by three different beam angles of the 256-ch phased array system.

carried out using the electrical element scanning capability of the phased array system, which selects the partial elements as the transmitting or receiving element. Fig. 13 shows the concept of the phased array TOFD technique and a typical CRT display in the on-line data acquisition mode. The TOFD B-scan display is obtained by the electrical array element scan without mechanical scanning perpendicular to the weld line. Only by a mechanical scan in the direction of weld line can both D-scan and B-scan images be obtained. Thus, a high-speed inspection (defect detection) and precise inspection (defect sizing) can be achieved using this technique.

Fig. 14 shows examples of phased array TOFD inspection results for the sizing of far surface and near surface breaking EDM slots prepared in the parent materials. It is recognized that the phased array TOFD technique has good capabilities for crack depth sizing. Fig. 15 also shows examples of phased array TOFD inspection results for near surface breaking EDM slots prepared in the HAZ region of a weldment. The interrupt of lateral wave is observed by the near surface breaking slots. From the top of arc coinciding with the bottom tip of slot, the depth of the slot tip is calculated. Fig. 16 shows the sizing accuracy of the depth of the slot tip by the phased array TOFD technique. In this case, the accuracy of 1 mm has been obtained for the welded specimen.

Fig. 17 shows a phased array TOFD B-scan image for the SCC, which is opened at the far surface. The locus of tip diffraction echo at the each tip of SCC can be clearly observed. The real size of SCC in these specimens is not measured by cutting, so TOFD results were compared to the measured SCC depth at both sides of the specimen surfaces. Fig. 18 compares TOFD sizing

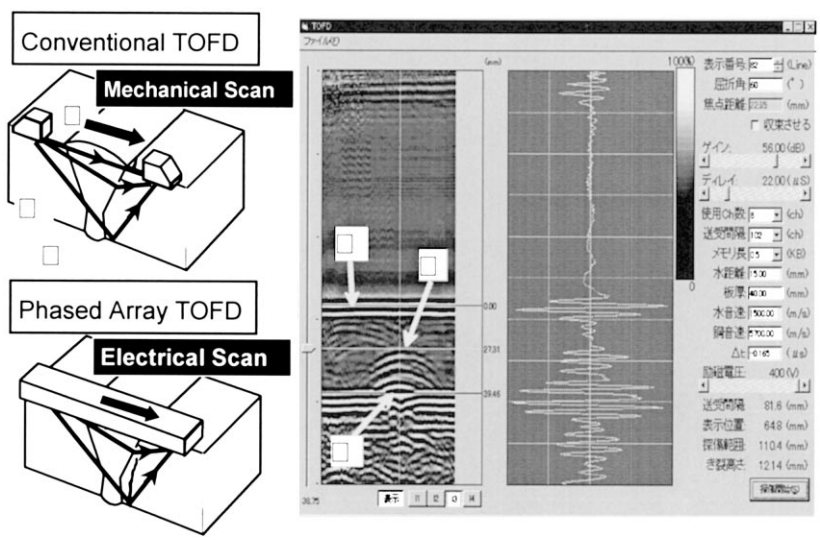

Fig. 13. Concept of phased array TOFD technique and typical CRT display of on-line data acquisition mode.

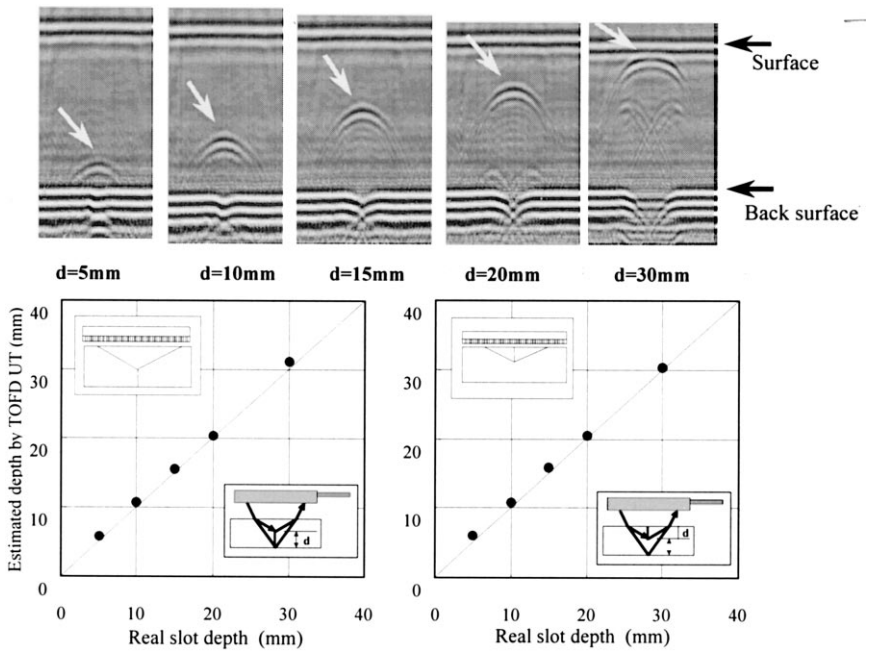

Fig. 14. Results of crack sizing experiment by phased array TOFD on both near-surface and far-surface breaking slots.

results for SCC and real SCC depth measured on the specimen side surface. A good agreement has been observed in these results, though the real depth of SCC on both side surfaces is slightly different.

2.4. Mock-up test of the 256ch phased array system

Two types of mock-up tests with the phased array system have been conducted in order to ensure that a developed phased array system could be applied to the real core shroud in the BWR plant.

Fig. 19 gives an overview of the mock-up test stand that can be used in the laboratory. This mock-up stand has a water jacket for the phased array immersion test and has a specimen that is attached in the wall of the shroud.

As shown in Fig. 20, a realistic mock-up test has been conducted in the training-pool facility, which is used for multi-purpose experiments such as verification tests for developed maintenance equipment. This test facility has the partially full size of the actual core shroud, and has an inner hole or outer core shroud component. The scanning device of the phased array probe runs on top of the shroud, and the arm of the scanning device

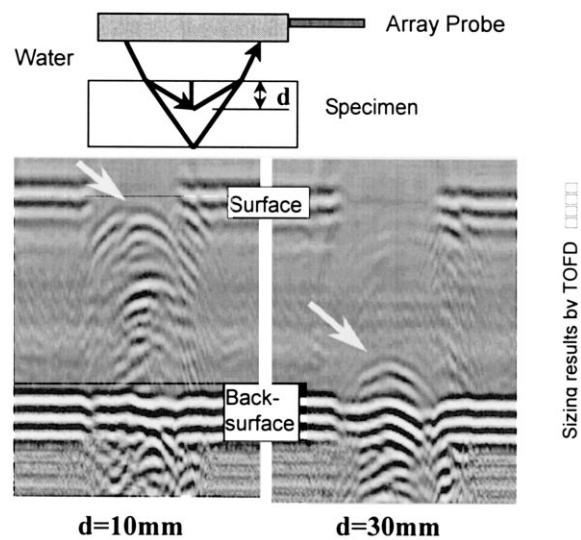

Fig. 15. Examples of phased array TOFD for the sizing of surface opened EDM slots.

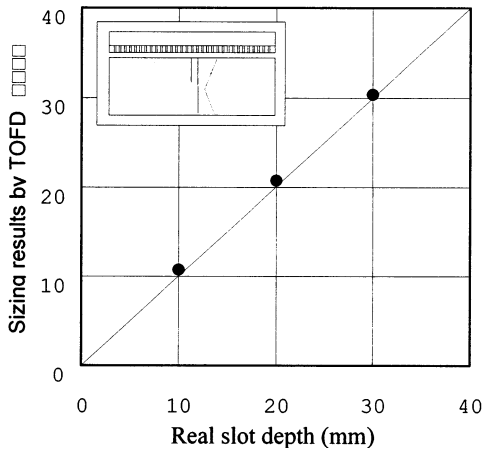

Fig. 16. Defect depth sizing accuracy of phased array TOFD for the surface opened EDM slots.

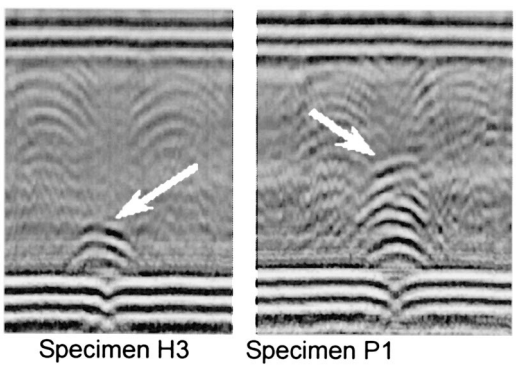

Fig. 17. Phased array TOFD B-scan imaging results for SCC on the far surface.

brings the array probe into the position of weldment. The test specimen, which has EDM slots, is attached to the wall of the shroud.

As for the results of these mock-up tests, it is recognized that the defect detection and sizing capabilities of the 256ch phased array system are the same as those under laboratory conditions.

3. Development of the potential drop method for surface crack sizing

3.1. New approach for the potential drop method

Ultrasonic examination has superior features such that the defect in the mid-section of the plate and the defect on the opposite side of plate can be detected. However, it is not that ultrasonic examination is suitable for detecting the whole defects and for use with whole materials. It is well known that the detection of defects through the weldment of austenitic stainless is not easy and that a rough surface is not suitable for a reliable inspection. Sometimes in such a case, an electromagnetic inspection technique such as the potential drop method or eddy current method is suitable for defect detection and sizing. For this purpose, a new and improved potential drop method has been developed.

The potential drop technique uses four contacting pins that are arranged in the same line and used for a current supply and measurement of potential difference. In one of the conventional potential drop methods, a pair of outer pins for current supply is set at a relatively distant position in order to make a uniform current field in the objective material. Another pair of inner pins are attached near the crack and are used for measuring the potential drop. This configuration of contact pins allows a theoretical analysis based on the uniform field theory (Johnson, 1965). Another conventional potential drop method uses a contact pin arrangement with the same distance in

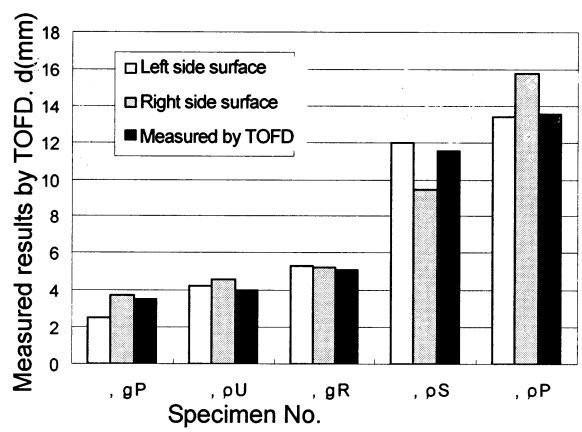

Fig. 18. Comparison between TOFD results and real SCC depth on the specimen's side surface.

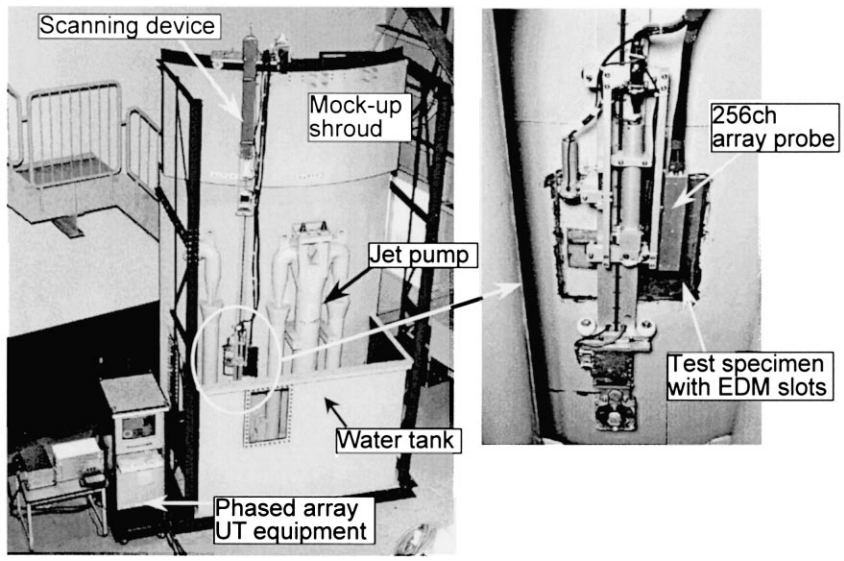

Fig. 19. Mock-up test of phased array system and scanning device.

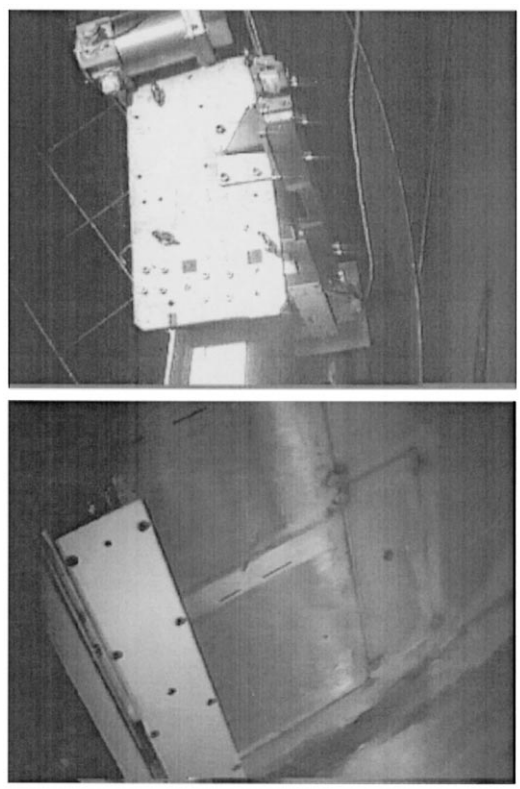

(a) Scanning device and its arm on the top of shroud.

(b) Phased array probe and the specimen which contains near surface and far surface breaking EDM slots in the shroud wall.

Fig. 20. Realistic application of phased array system in the Training pool facility.

each pin. This configuration is used in commercial equipment. Usually in this case, a calibration procedure is required to determine the crack depth and shape of the objective materials.

Recently, a new technique has been developed, in which the closely coupled probes for current supply pin and potential measurement pin are used (Saka et al., 1998). In this technique, the calibration equation, which relates the potential drop to the crack depth and the crack length, is derived in which a finite element method (FEM) is utilized.

3.2. Procedure of theoretical calibration equation

The problem of current flow in a material is governed by the Laplace equation as

$$\nabla^2\phi = 0 \tag{1}$$

where ϕ is the electrical potential and ∇^2 is the 3-D Laplace operator. Eq. (1) can be solved by using FEM to obtain ϕ, where the crack surfaces are assumed to be insulated electrically.

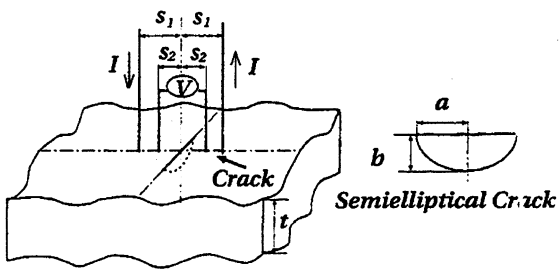

Fig. 21. Model of 3-D surface crack.

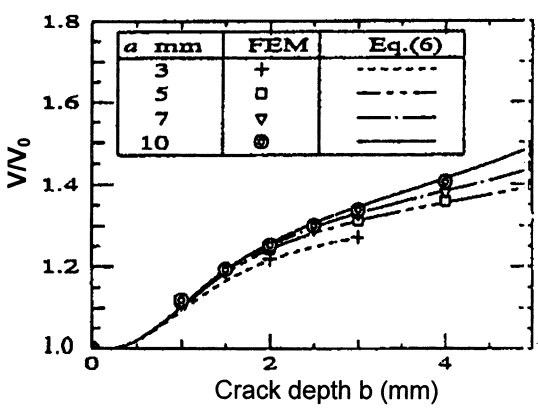

Fig. 22. Potential drop calculation by FEM and its estimate equation.

Consider a 3-D problem of measuring semi-elliptical cracks on the surface of an infinite plate, as shown in Fig. 21, where t is the plate thickness, $2a$ the crack length, and b the maximum crack depth. The constant d.c. current, I, is applied between two points, which are at a distance s_1 away from the crack respectively, on the cracked surface. The potential drop, V, is measured between two points that are at a distance of s_2 from the crack, respectively, within the positions of the current input and output points.

The relation of the potential drop to the crack size is obtained by using the FEM, when the half crack length, a, is larger than the crack depth, b, and b is smaller than t, because these conditions are typical for a crack. The following value was used as a probe parameter; $s_1 = 1.5$ mm and $s_2 = 1$ mm. In Fig. 22, symbols are FEM results, which shows the correlation between crack depth and potential drop with crack, in the different crack length condition. The potential drop with the crack is normalized by the potential drop without a crack. Furthermore, the curves are derived by the following equations:

$$\frac{V}{V_0} = \left\{ F\left(\frac{b}{s_2}\right) \times D\left(\frac{a}{s_2}, \frac{b}{a}\right) + 1 \right\} \times C(a,\ b,\ s_2,\ t) \tag{2}$$

where

$$F\left(\frac{b}{s_2}\right) = \ln\left[\frac{\ln\left\{ \left(\alpha \frac{b}{s_2} \right)^{\beta} \right\} + 1}{\gamma} \right] \times \zeta \tag{3}$$

$$D\left(\frac{a}{s_2}, \frac{b}{a}\right) = \exp\left[-\delta \left(\frac{a}{s_2}\right)^{-\zeta} \left(\frac{b}{a}\right)^{(\eta(a/s_2)+\varphi)} \right] \tag{4}$$

$$C(a,\ b,\ s_2,\ t) = \begin{cases} \left(\lambda \frac{s_2}{t}\right)^{\kappa} \frac{a}{s_2} \left(\frac{b}{t}\right)^3 + 1 (\text{for } a \le 20\ \text{mm}) \\ \theta \left(\frac{s_2}{t}\right)^{\chi} \frac{b}{t-b} + 1 (\text{for } a = \infty) \end{cases} . \tag{5}$$

In these equations, each α, β, γ, ξ, δ, ζ, η, φ, λ, κ, θ, χ, ω, and ν is a numerically decided parameter. A good correlation between the FEM results

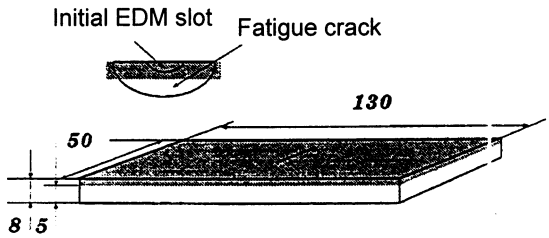

Fig. 23. Fatigue cracked specimen for potential drop measurement.

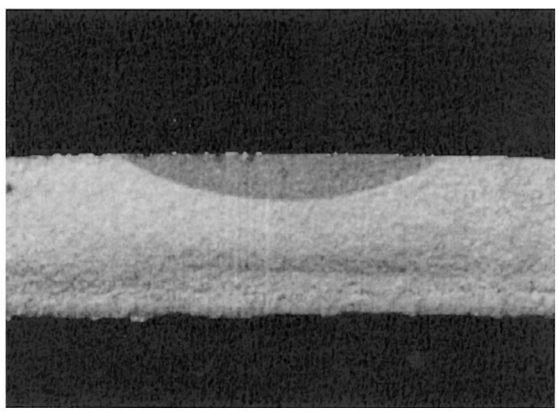

Fig. 24. An example of fractured surface of fatigue specimen.

(symbols) and the numerical equation is observed in Fig. 22.

3.3. Experimental results on fatigue-cracked specimens

An experiment on the potential drop method was carried out on the fatigue-cracked specimens. A semi-elliptical EDM slot was prepared on the specimen surface, and this specimen was loaded by a fatigue machine. After the fatigue-crack growth had occurred, the initial EDM slot was removed, as shown in Fig. 23, and then this specimen was used for the potential drop measurement. After the potential drop had been measured, the heat tint was conducted, and then specimens were broken by fatigue loading. The actual fatigue crack depth and measured value were compared.

Fig. 24 shows an example of a fractured surface. Fig. 25 shows the closely coupled probe and the equipment of potential drop measurement, which were developed in this work.

The final results for the evaluation of potential drop method are described in Fig. 26. Both the measured value of crack depth by the potential drop method and the actual crack depth show a good agreement with each other. On this figure,

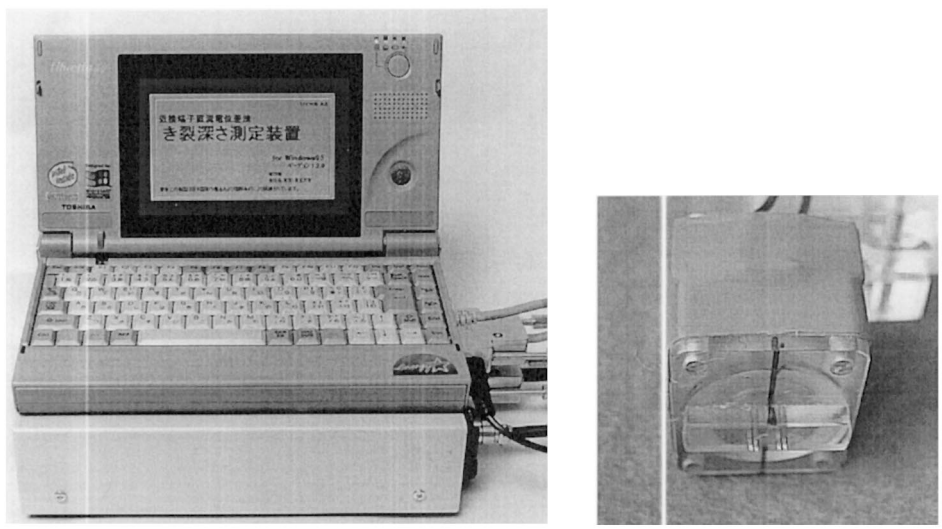

Fig. 25. Closely coupled probe and potential drop measurement equipment.

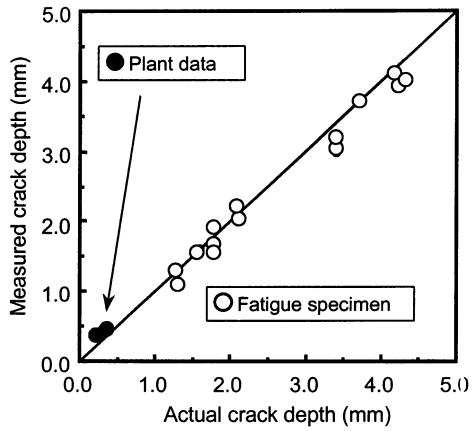

Fig. 26. Correlation between actual crack depth and measured crack depth by potential drop method.

the actual crack data obtained in the structural component of the plant are plotted. It is recognized that the newly developed potential drop method has good capabilities for crack-depth sizing. Furthermore, good results have been obtained for the SCC cracks in the HAZ region of a stainless-steel weldment.

4. Conclusion

The water gap phased array technique has been improved for use in the inspection of a core shroud weldment. First of all, a 256-channel phased array probe and array system had been developed for the purpose of high-speed inspection, which minimizes mechanical scanning. After the basic experiment for determining suitable beam control conditions for the normal beam and angle beam linear scanning operation, defect detection capabilities were examined on the EDM slot specimen and the SCC specimens of a core shroud weldment. Furthermore, the TOFD inspection technique can be carried out using an electrical element scanning capability, which selects the partial elements as the transmitting or receiving element. As for the results of these experiments, it has been shown that the water gap phased array method is effective for detecting and sizing the defect by the simultaneous B-scan imaging of three different beam incident directions, and by the phased array TOFD technique. A realistic mock-up test was carried out in the training-pool facility, and the capabilities of the developed phased array system were found to be the same as those in the laboratory.

The potential drop crack depth sizing method has been improved in order to enhance the sensitivity of the potential drop change with the change in crack depth and in order to perform the crack-depth sizing procedure, which is not required to make calibration curves for each crack and material by the numerical approach. The accuracy of this newly developed potential drop method was evaluated on fatigue-cracked specimens, and this method was found to be effective for real cracks in an actual component.

References

Fischer, K., et al., 1988. Proc. 9th Int. Conf. NDE in the Nuclear Industry, p. 29.
Johnson, H., 1965. Mater. Res. Stand. 5 (1), 442.
Komura, I., et al., 1985. Nucl. Eng. Design 87, 185.
Komura, I., et al., 1986. Proc. 8th Int. Conf. NDE in the Nuclear Industry, p. 591.
Komura, I., et al., 1996. Proc. 14th Int. Conf. NDE in the Nuclear Industry, p. 305.
Uchida, K., et al., 1984. Nucl. Eng. Design 81, 309.
Saka, M., et al., 1998. Trans. ASME. J. Pressure Vessel Technol. 120, 376.
Wustenberg, H., et al., 1988. Proc. 9th Int. Conf. NDE in the Nuclear Industry, p. 97.